

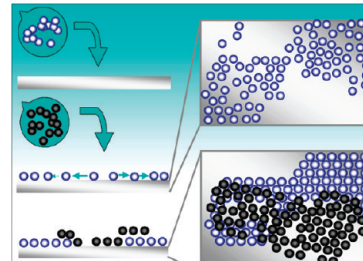
How the Level of Ordering of 2D Nanocrystal Superlattices Is Controlled by Their Deposition Mode

Emilie Klecha, Dorothée Ingert, and Marie P. Pilani*

Laboratoire L.M.2.N., UMR C.N.R.S 7070, Université P. et M. Curie (Paris VI), B.P. 52, 4 Place Jussieu, F-752 31 Paris Cedex 05, France

ABSTRACT Here, we show that droplet deposition of 5 nm Ag nanocrystals induces the formation of two bidimensionnal arrays differing by their level of long-range ordering. This is valid for the alkanethiol/solvent combinations using decanethiol or dodecanethiol as the coating agent and hexane, octane, decane, or dodecane as the solvent to disperse the nanocrystals. The spacing between the nanocrystals does not diverge from one network to the other for a given combination but depends conversely on this combination. This is demonstrated by employing an intrinsic property of highly ordered Ag nanocrystals subjected to oxygen plasma and also classical methods usually used for this purpose.

SECTION Nanoparticles and Nanostructures



A challenging requirement for future devices is to process a wide range of increasingly smaller materials. Nanomaterials have received much attention lately for their promising potential in many domains (optics,^{1,2} mechanics,³ biology,^{4,5} and so forth), arising from their unique properties that are different from both those of the bulk material and those of the isolated nanocrystals. An ultimate goal in nanotechnology for years has thus been to control the size and morphology (structure and shape) either of the nanocrystals or of their arrangements into two and three dimensions. The nanocrystal ordering in these assemblies is a crucial parameter in the control of physical properties and especially in the collective physical properties.^{6–9} The distance separating the nanocrystals is also of major importance in these materials. Indeed, different electrical behaviors such as insulator-to-metal transition have been reported to depend on this internanocrystals distance.^{10–12} The most commonly used way to create ordered architectures at the nanometer scale is the spontaneous self-assembly phenomenon.¹³ The first self-organizations were obtained 15 years ago by droplet deposition of colloidal solutions onto a substrate.^{14,15} Spherical nanocrystals ordered in 2D hexagonal networks have been observed over a large scale. The densest 2D packing for spheres is hexagonal and thus the one energetically favored. However, the patterns exhibit a nonuniform particle distribution on the substrate surfaces, testifying to convection flows and solvent fluctuation during the evaporation. Numerous studies either experimental or theoretical have thus been carried out to understand and to improve either the ordering or the scale of the self-assemblies.^{16–26} In most cases, it is considered as a competition between the diffusion of the nanocrystals and the solvent dewetting occurring at the liquid/substrate interface. When the particle diffusion speed in the colloidal solution is slower than the solvent evaporation speed, the particle concentration

increases underneath the liquid surface, and capillary forces, due to the surface tension, drive the assembly into a 2D array (i.e., a monolayer).^{25,26} Nonetheless, it has been shown that under defined conditions of one-drop deposition, the process arises at the liquid/air interface²⁷ or even in the bulk solution.²⁸ When the solvent is completely evaporated, most often the internanocrystal distances are smaller than two lengths of the ligand molecules adsorbed at the nanocrystal surfaces, and interdigitation of these molecule tails is then commonly assumed. These organizations are so-called crystallized by analogy with molecular crystallization. This indicates a strong stability of the interdigitated tail structures after the solvent dewetting and provides self-ordered nanocrystals with intrinsic chemical properties. Indeed, 2D Ag nanocrystal superlattices with a high level of ordering subjected to oxygen plasma remain unchanged, whereas the same nanocrystals with lower orders coalesce into large silver crystals without any silver oxide derivatives.²⁹ Similarly, self-ordered Co nanocrystals exposed to air for a few hours evolve to a core–shell $\text{Co}_{\text{hcp}}/\text{CoO}$ self-assembled structure, whereas the same nanocrystals isolated on the substrate are entirely transformed in pure CoO nanoparticles.^{30,31}

Here, we demonstrate that two types of nanocrystal ordering are systematically obtained by the droplet deposition of 5 nm Ag nanocrystals coated with different alkanethiols and dispersed in various solvents. The internanocrystal distance of the 2D arrays is not related to their ordering and differs with the combination alkanethiol/solvent.

Silver nanocrystals coated with either dodecanethiol ($\text{C}_{12}\text{H}_{25}\text{SH}$) or decanethiol ($\text{C}_{10}\text{H}_{21}\text{SH}$), designated $\text{Ag}-\text{C}_{12}$

Received Date: March 30, 2010

Accepted Date: April 29, 2010

and Ag–C₁₀, respectively, are synthesized via the reverse micellar system (see Experimental Section). At the end of the synthesis, the Ag nanocrystals are dispersed in hexane (C₆H₁₄) and deposited as is, or the hexane is evaporated, and the nanocrystals are dispersed in another solvent such as those used here, octane, decane, or dodecane. Two 10-μL drops (at 1×10^{-3} mol·L⁻¹) of Ag–C₁₀/octane nanocrystals are deposited successively on a copper transmission electron microscopy (TEM) grid covered by highly oriented pyrolytic graphite (HOPG) with a filter paper underneath. At low magnification, the TEM image in Figure 1A shows a 2D monolayer (areas marked 1 and 2) ordered over a large scale and bilayers. The fast fourier transform (FFT) of the area 1 of the monolayer shows two hexagons related to first and second order (inset 1 Figure 1A), attesting to a well-defined hexagonal network ordered over a long range. Conversely, the adjacent area of the monolayer marked 2 exhibits hexagonal arrangements with many local defects such as nanocrystal vacancies, grain boundaries, and distortions, scattered all over the area that is shown on its corresponding FFT by the presence of two diffuse rings without any defined spots (inset 2, Figure 1A). In both cases (areas 1 and 2), the average nanocrystals size (5 nm) and distribution (9 %), determined using a minimum of 500 nanocrystals per area, are identical. This indicates that no size segregation change occurs from one network to the other during the deposition process and that a small size dispersion is not the only parameter obtain by well-ordered monolayers, as usually claimed. The mean distance separating edge-to-edge well-aligned nanocrystals (d_{p-p}) in the two hexagonal networks (see the alignments Figure 1A) has been measured³² and remains unchanged at $d_{p-p} = 2.2 \pm 0.1$ nm. Thus, the deposition of Ag–C₁₀/octane nanocrystals leads to the formation of two 2D networks (i.e., monolayers) of the same compactness, differing by their level of long-range ordering. This difference cannot be attributed to HOPG surface defects (bundles, steps, and/or islands) due to its cleavage because the range of defect-free domains is in μm²,³³ which is higher than that of the obtained monolayer areas. Octane has a low boiling point (T°b) that entails a fast evaporation, especially under our experimental conditions (i.e., with a filter paper underneath of the TEM grid). Also, short alkanethiols (i.e., C ≤ 10) are known to present more defects in their tails than their homologues with a longer tail^{34,35} (i.e., C ≥ 12), and these can hinder nanocrystal ordering. Hence, in order to evaluate the influence of the solvent evaporation rate and of the alkanethiol tail defects in these results, the same depositions (two successive 10 μL drops at 1×10^{-3} mol·L⁻¹) have been performed with Ag–C₁₀ nanocrystals from the mother solution (i.e., dispersed in hexane, which has a lower T°b), with Ag–C₁₀ nanocrystals dispersed in decane and dodecane characterized by a higher T°b, and finally, with Ag–C₁₂ nanocrystals dispersed in the same four solvents. In each case (i.e., combination alkanethiol/solvent), the TEM image shows systematically two types of monolayer areas with different long-range levels of ordering and bilayers,³⁶ as above for Ag–C₁₀/octane. The corresponding FFT areas show either well-defined hexagons or two diffuse rings or, at least, very diffuse spots indicating the presence of more defects. From these results, it is concluded that neither the evaporation

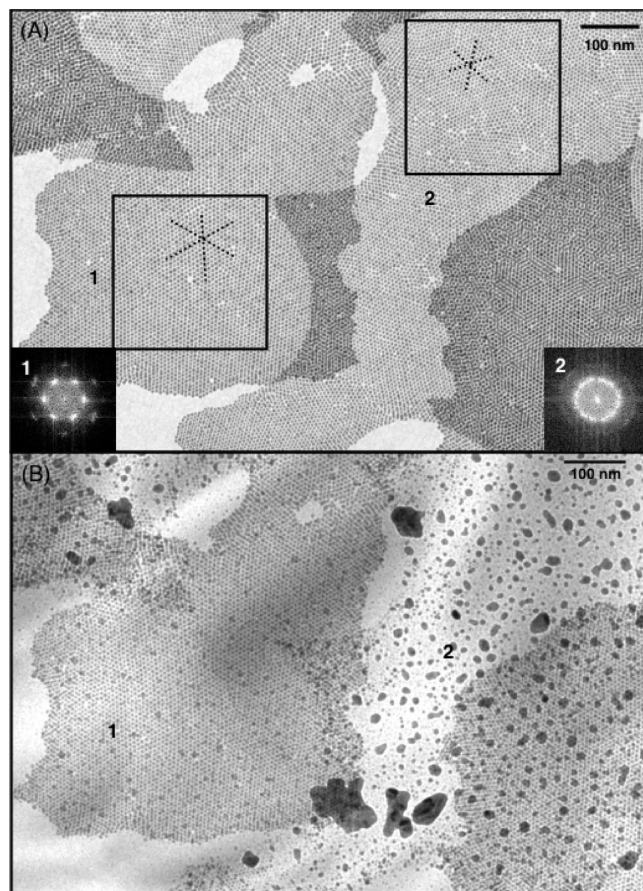


Figure 1. Transmission electron microscopy (TEM) image at low magnification of silver nanocrystals coated with decanethiol and dispersed in an octane (Ag–C₁₀/octane) droplet deposited on highly oriented pyrolytic graphite (HOPG) (A) before and (B) after plasma treatment at 10 W for 5 s. Fast fourier transform (FFT) of the black square area (left inset) 1 and (right inset) 2.

rate nor the coating tail defects play a role in the difference in nanocrystal orderings, and two types of monolayers are definitely obtained.

Conversely and surprisingly, the internanocrystal distance given Figure 2A, as a function of the number of carbon atoms in the alkyl solvent chain, depends on the solvent used and follows the same behavior for both coating agents. Note that the d_{p-p} in both networks is similar, except for Ag–C₁₂/hexane,²⁹ and its variation from one solvent to the other is significant compared to the experimental error. The d_{p-p} decreases upon increasing the solvent chain length, reaches a minimum that depends on the thiol used, and finally increases for a longer solvent chain. This is in contradiction with several papers from which this spacing is controlled by the alkanethiol chain length independently of the used solvent.^{9,17,24,25,37,38} A further characterization of these systems with SAXS could help us to understand such behavior. Nevertheless, the experimental conditions, a small amount of material deposited on a TEM grid, are inappropriate for such experiments. However, the similar behavior for both coating agents could indicate that the same phenomenon takes place. A competition between the solvent evaporation and the

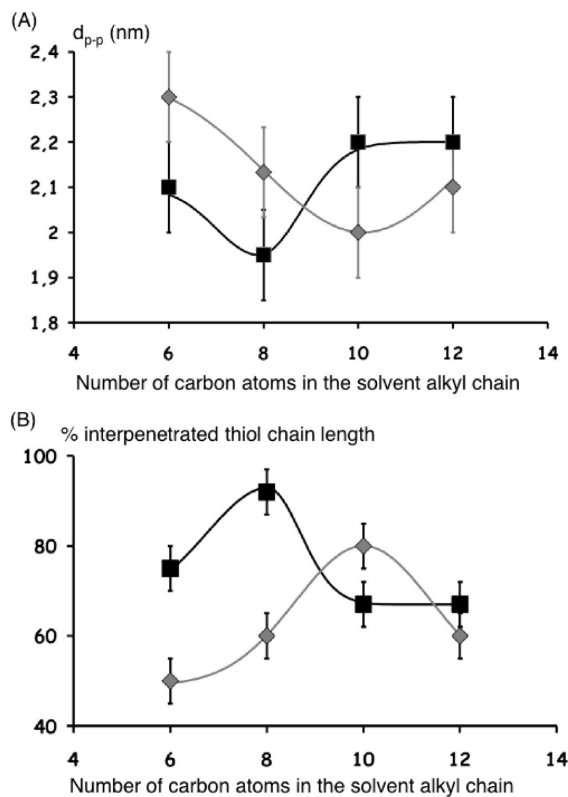


Figure 2. (A) Average of the internanocrystal distances measured in the three directions of the higher ordered networks obtained with the Ag-C_{10} (♦) and Ag-C_{12} (■) nanocrystals dispersed in the four solvents as a function of the number of carbon atoms in the solvent alkyl chain. (B) Percentage of (♦) decanethiol and (■) dodecanethiol length tails interdigitated corresponding to the different d_{p-p} measured as a function of the number of carbon atoms in the solvent alkyl chain.

swelling of the thiols occurs and probably differs with the used alkanethiol/solvent combination, which explains the presence of the minima (for more information, see ref 39). The percentage of interpenetrated thiol lengths related to each d_{p-p} can be estimated from the decane- and dodecanethiol lengths (1.6 and 1.8 nm, respectively, taking into account the polar head group and assuming that the chains are in a trans configuration). Figure 2B gives these percentages and shows that they are greater in most of the cases for dodecanethiol, although its length is longer than that of decanethiol. This could be attributed to the fact that dodecanethiol tails are better organized than those of decanethiol. Thus, the soft adjacent coronas can easily and more deeply interpenetrate than decanethiol ones having more gauche defects. The increase in the solvent length favors a better organization of the decanethiol tails due to the longer evaporation time and extends the interdigitation up to a maximum (i.e., a d_{p-p} minimum), shifted from octane (C8) to decane (C10) when dodecanethiol (C12) is replaced by decanethiol (C10). To confirm that these systems are at the equilibrium state, Ag-C_{12} /octane nanocrystal networks were annealed at 380 K for 2 h and then at 700 K. The nanocrystals and the networks remained unchanged without any coalescence (Figure S11, Supporting Information). This clearly shows that

the increase in the chain mobility to 65–75%,⁴⁰ to favor the diffusion of the nanocrystals and to reach the equilibrium state in the annealing process,⁴¹ does not play any role in the d_{p-p} value nor in the superlattice integrity. One can conclude that the nanocrystals are in a stable energetic configuration and reach their equilibrium state during the evaporation process and self-order into two arrays with different levels of ordering. From a previous study we know that when highly ordered nanocrystals are subjected to an oxygen plasma treatment (10 W, 5 s) generated by a reactive ion etching process, they are quite immune, whereas when defects are present, large Ag crystals are formed.²⁹ Figure 1B is the TEM image of the same area in Figure 1A of Ag-C_{10} /octane after plasma treatment. Monolayer 1 with a high level of ordering is rather intact, while monolayer 2, with a lower level of ordering, and the upper layer of the bilayer are completely destroyed, exhibiting the homogeneous coalescence of all of the nanocrystals forming larger particles. The various alkanethiol/solvent combinations follow strictly this behavior³⁶ (Figure S12, Supporting Information), confirming that the stability does not depend on the d_{p-p} values but on the level of nanocrystal ordering. Moreover, the sizes and size distributions of the coalesced objects from the bilayers and the monolayer 2 are identical.^{29,36} This indicates that the coalescence mechanism is similar whether the nanocrystals are initially deposited on the bare substrate (i.e., monolayer 2) or on a nanocrystals layer (i.e., upper layer of the bilayers). It seems from a careful observation of the samples after plasma treatment that monolayer 2 and the upper layer of the bilayer behave as the one and only monolayer, which is also supported before plasma exposure.

Figure 3A shows the TEM image of a Ag-C_{12} /octane deposit. Monolayer 1 is well-ordered in the hexagonal network, whereas monolayer 2 is less ordered, as is confirmed by the higher magnifications (Figure 3B and C) and by their corresponding FFT in the inset. The bilayer pattern exhibits a flower-like structure that does not correspond to a compact (i.e., fcc or hcp) packing of two nanocrystal layers expected in the case of a layer-by-layer growth. The reconstructed fcc or hcp patterns made of the superposition of two monolayer 1 networks (Figure 3E) and two monolayer 2 networks (Figure 3F) exhibit straight-line patterns that markedly differ from the flower-like bilayer pattern (Figure 3D). At the opposite, the pattern obtained by the superposition of monolayer 1 and 2 networks (Figure 3G) exhibits a flower-like pattern close to that one observed on the samples (Figure 3D). Thus, this tends to prove that the bilayer is made by the superposition of the monolayers 1 and 2, meaning that monolayer 2 and the upper layer of the bilayer are the one and only monolayer superimposed on the monolayer 1. To support this explanation, we have to consider the deposition process, two successive drops of the colloidal solution on the TEM grid deposited on a filter paper, and the results of Bigioni et al.²⁷ showing the formation of 2D nanocrystal assemblies at the liquid/air interface. An excess of alkanethiol is added to the colloidal solution, and a drop is deposited onto a substrate. The free ligands reach the liquid/air interface and attract the coated nanocrystals. With the solvent evaporation, a nanocrystal film is formed at this interface, leading finally to a dense packing monolayer on the substrate. In our experiments, the alkanethiol

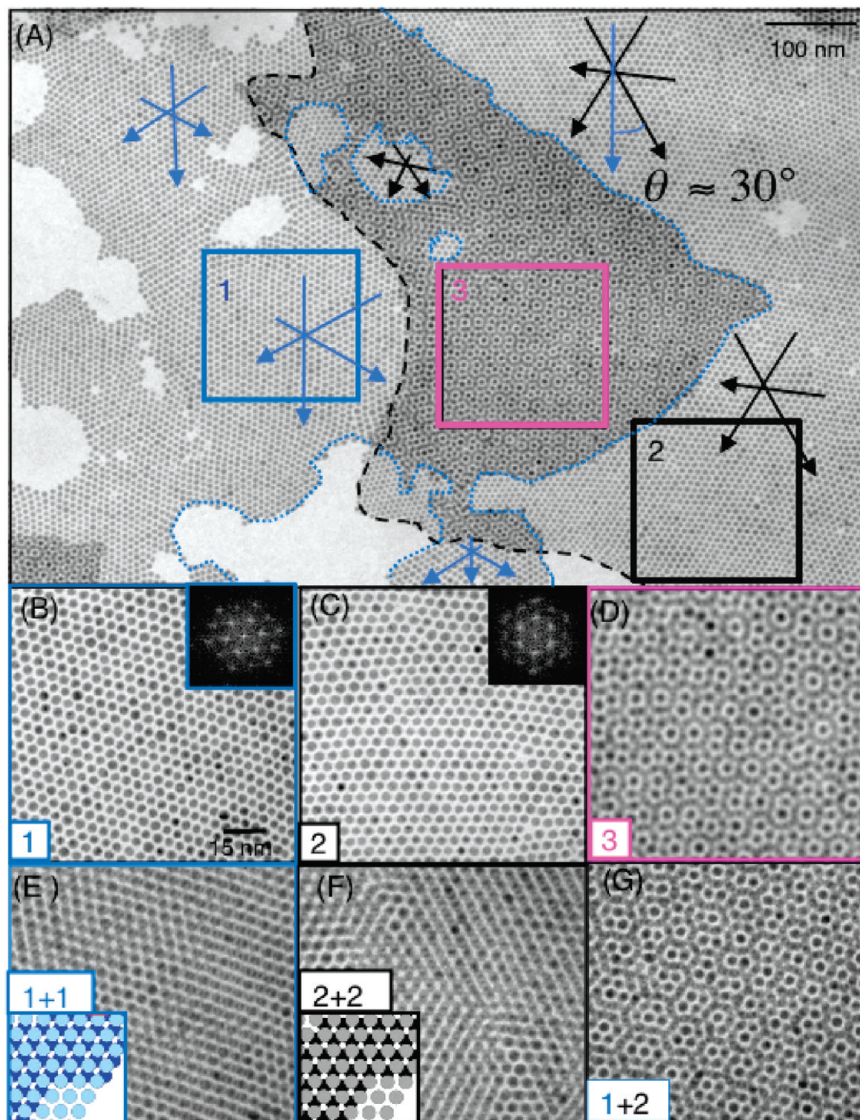


Figure 3. TEM images of Ag–C₁₂/octane deposited on HOPG at (A) low magnification and higher magnifications of the monolayers marked (B) 1 and (C) 2 and (D) of the bilayer. The reconstructed fcc pattern made of two superposed monolayers, (E) 1 and (F) 2, and of the superposed networks, (G) 1 and 2. The scale bar in (B) applies for (B–G).

concentration added is very large, and free alkanethiols probably remain in the final solution even after washing. Then, the first drop induces the formation of one monolayer at the liquid/air interface. The paper underneath the TEM grid favors the expulsion of the solvent keeping ordered monolayer areas. Nearly at the end of evaporation, because of the particle/substrate interactions, the monolayer is stuck on the very flat substrate surface (TEM grid covered by HOPG) and has coverage defects such as holes in the particle pattern film due to convection flux. The second drop is added and induces in parallel the formation of the second monolayer at the new liquid/air interface. Here again, the solvent evaporates and is absorbed by the filter paper. When the particle substrate interactions are predominant, the second film of nanocrystals is pinned on the surface already covered by the first monolayer, presenting coverage defects. The nanocrystals forming the first monolayer are pinned on a flat surface and

benefit from more time to diffuse on the substrate surface, giving finally a higher level of ordering. Indeed, the addition of the second drop increases the thiol tail mobility, which improves the nanocrystals ordering. This is confirmed by the fact that one monolayer with defects⁴² is obtained by only one-drop deposition of the colloidal solution (Figure 4A) and that a higher-ordered monolayer is obtained by the deposition of one drop of the colloidal solution followed by one drop of pure solvent (Figure 4B). The second monolayer is stuck on a rougher surface with free nanocrystals and monolayer domains, which do not allow as much diffusion as in the case of the first monolayer and probably modify the solvent wetting on the surface.⁴³

This model (Scheme 1) explains the two levels of long-range ordering systematically observed for any evaporation rate. These results show that independently of the alkanethiol/solvent combination, the droplet deposition induces

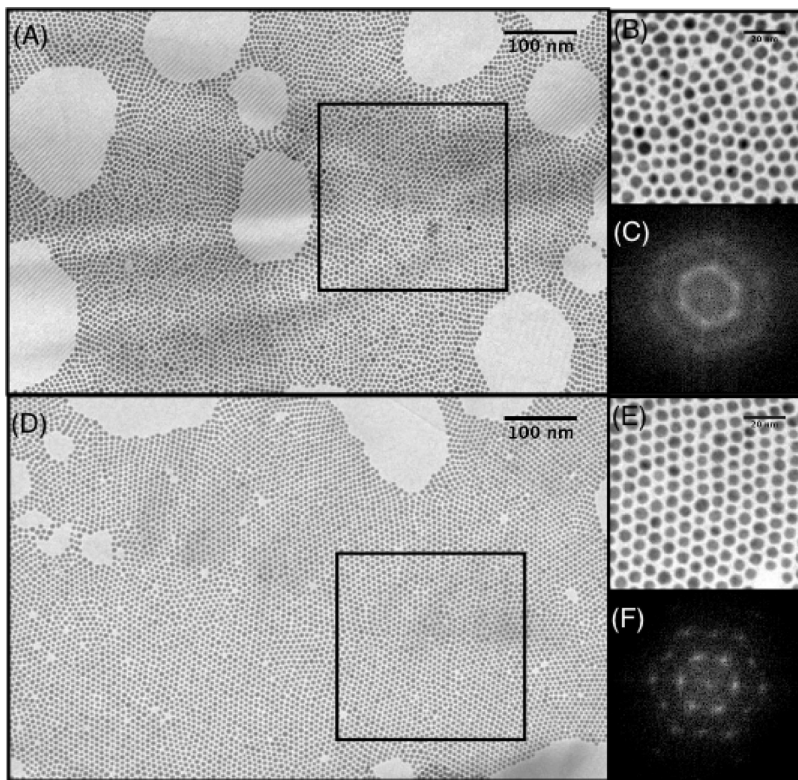
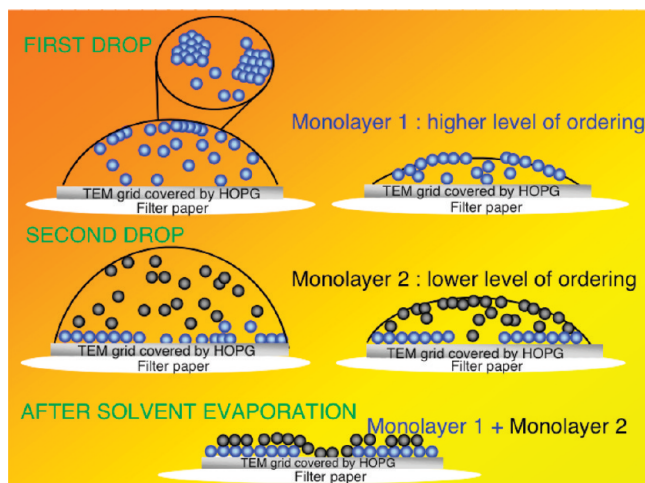


Figure 4. Transmission electron microscopy (TEM) images at (A) low and (B) higher magnification of only one drop of $\text{Ag}-\text{C}_{12}$ /hexane deposited on a TEM grid covered by HOPG. (C) FFT corresponding to the black square in (A). TEM images at (D) low and (E) higher magnification of the deposit obtained by one drop of $\text{Ag}-\text{C}_{12}$ /hexane solution followed by one drop of hexane on a TEM grid covered by HOPG. (F) FFT corresponding to the black square in (D).

Scheme 1. Evaporation Process at Different Stages with the Formation and the Growth of the 2D Assemblies for the Used Droplet Deposition



the formation of two 2D arrays with different levels of ordering but with the same compactness that is, conversely, controlled by this combination.

In conclusion, self-assemblies of 5 nm silver nanocrystals coated either with decanethiol ($\text{Ag}-\text{C}_{10}$) or dodecanethiol ($\text{Ag}-\text{C}_{12}$) and dispersed in four different alkane solvents, hexane, octane, decane, and dodecane, have been studied.

It has been shown that the two-drop deposition leads to the formation of monolayers and bilayers. The 2D arrays are systematically divided into two monolayers with the same compactness but with different levels of ordering for any used thiol/solvent combination. The internanocrystal spacing of the 2D networks has been carefully studied, and it has been shown that the ligand tail length is not the only factor involved in its tuning and that it is controlled by the used alkanethiol/solvent combination. A mechanism based on the formation of the monolayers at the liquid/air interface with each drops inducing two levels of ordering has been proposed and is strongly supported by the characterization of the deposits either before or after oxygen plasma treatment.

EXPERIMENTAL SECTION

Silver nanocrystals are obtained by mixing two reverse micelle solutions.⁴⁴ The first is 60% 0.1 M $\text{Ag}(\text{AOT})$ and 40% 0.1 M $\text{Na}(\text{AOT})$ dissolved in isoctane. The water content, $w = [\text{H}_2\text{O}]/[\text{AOT}]$, is kept at 2. The second solution is 0.1 M NaAOT in isoctane with water replaced by hydrazine. Hydrazine is in excess and its content, defined as $[\text{N}_2\text{H}_4]/[\text{AOT}]$, is kept at 1.44. Immediately after mixing these two reverse micelle solutions, silver nanocrystals are formed. The coating agent (dodecanethiol or decanethiol) is then added to the reverse micelles solution containing the nanocrystals. Ethanol is then added to the solution to remove the AOT surfactant. After a size selection process, the nanocrystals are characterized by a

mean diameter of 5.0 nm with a size distribution of 9 % and are dispersed in hexane (C_6H_{14}). The nanocrystals are fcc crystals with three different shapes,⁴⁵ decahedra, icosahedra, and cubooctahedra.

Electron micrographs are obtained with a JEOL Model JEM 100CX electron microscope.

After deposition of the nanocrystals solution on the TEM grids, the samples are loaded into the RIE apparatus. The reactive ion etching system is a Plassys MG 200. The plasma treatment is carried out using oxygen as the etching gas. The plasma power is 10 W, the exposure time is 5 s, the working pressure is maintained at 6.4 μ bar, and the oxygen flow rate is 10 sccm.

SUPPORTING INFORMATION AVAILABLE Transmission electron microscopy (TEM) images of the Ag–C₁₂/octane deposit before and after annealing at 380 K after 2 h and after annealing at 700 K and TEM images of Ag–C₁₂/decane before and after plasma treatment (10 w, 5 s). This material is available free of charge via the Internet at <http://pubs.acs.org>.

AUTHOR INFORMATION

Corresponding Author:

*To whom correspondence should be addressed. E-mail: marie-paule.pileni@upmc.fr.

ACKNOWLEDGMENT The authors thank Dr. E. Vincent, Dr. C. Fermon, and Dr. P.F. Orfila (SPEC/DRECAM/CEA Saclay-France) for access to the clean room and lithography equipment, Professor Jacob Israelachvili (MRL/UCSB-USA), Dr. P. A. Albouy (LPS/Paris12-France), Dr. A. Courty (LM2N/Paris6-France), and Dr. I. Lisiecki (LM2N/Paris6-France) for fruitful discussions.

REFERENCES

- (1) Zaitseva, N.; Dai, Z. R.; Leon, F. R.; Krol, D. Optical Properties of CdSe Superlattices. *J. Am. Chem. Soc.* **2005**, *127*, 10221–10226.
- (2) Silly, F.; Gusev, A. O.; Taleb, A.; Charra, F.; Pileni, M. P. Coupled Plasmon Modes in an Ordered Hexagonal Monolayer of Metal Nanoparticles: A Direct Observation. *Phys. Rev. Lett.* **2000**, *84*, 5840–5843.
- (3) Mueggenburg, K. E.; Lin, X. M.; Goldsmith, R. H.; Jaeger, H. M. Elastic Membranes of Close-Packed Nanoparticle Arrays. *Nat. Mater.* **2007**, *6*, 656–660.
- (4) Firkowska, I.; Giannona, S.; Rojas-Chapana, J. A.; Luecke, K.; Brüstle, O.; Giersig, M. *Nanomaterials for Application in Medicine and Biology*; Springer: The Netherlands, 2008.
- (5) Gao, X.; Chan., W. C. W.; Nie, S. Quantum-Dot Nanocrystals for Ultrasensitive Biological Labeling and Multicolor Optical Encoding. *J. Biomed. Opt.* **2002**, *7*, 532–537.
- (6) Lalatonne, Y.; Richardi, J.; Motte, L.; Pileni, M. P. Influence of Short-Range Interactions on the Mesoscopic Organization of Magnetic Nanocrystals. *Phys. Rev. E* **2005**, *71*, 11404–11414.
- (7) Courty, A.; Mermet, A.; Albouy, P. A.; Duval, E.; Pileni, M. P. Vibrational Coherence of Self-Organized Silver Nanocrystals in f.c.c. Supra-Crystals. *Nat. Mater.* **2005**, *4*, 395–398.
- (8) Pileni, M. P. Self-Assembly of Inorganic Nanocrystals: Fabrication and Collective Intrinsic Properties. *Acc. Chem. Res.* **2007**, *40*, 685–693.
- (9) Puentes, V. F.; Krishnan, K. M.; Alivisatos, P. Synthesis, Self-Assembly, and Magnetic Behavior of a Two-Dimensional Superlattice of Single-Crystal ε-Co Nanoparticles. *Appl. Phys. Lett.* **2001**, *78*, 2187–2189.
- (10) Collier, C. P.; Saykally, R. J.; Shiang, J. J.; Henrichs, S. E.; Heath, J. R. Reversible Tuning of Silver Quantum Dot Monolayers Through the Metal–Insulator Transition. *Science* **1997**, *277*, 1978–1981.
- (11) Beecher, P.; Quinn, A. J.; Shevchenko, E. V.; Weller, H.; Redmond, G. Charge Transport in Weakly Coupled CoPt₃ Nanocrystal Assemblies. *J. Phys. Chem. B* **2004**, *108*, 9564–9567.
- (12) Quinn, A. J.; Beecher, P.; Iacopino, D.; Floyd, L.; De Merzi, G.; Shevchenko, E. V.; Weller, H.; Redmond, G. Manipulating the Charging Energy of Nanocrystal Arrays. *Small* **2005**, *6*, 613–618.
- (13) Prasad, B. L. V.; Sorensen, C. M.; Klabunde, K. J. Gold Nanoparticle Superlattices. *Chem. Soc. Rev.* **2008**, *37*, 1871–1883.
- (14) Motte, L.; Billoudet, F.; Pileni, M. P. Self-Assembled Monolayer of Nanosized Particles Differing by Their Sizes. *J. Phys. Chem.* **1995**, *99*, 16425–16429.
- (15) Murray, C. B.; Kagan, C. R.; Bawendi, M. G. Self-Organization of CdSe Nanocrystallites into Three-Dimensional Quantum Dot Superlattices. *Science* **1995**, *270*, 1335–1338.
- (16) Korgel, B. A.; Fullam, S.; Connolly, S.; Fitzmaurice, D. Assembly and Self-Organization of Silver Nanocrystal Superlattices: Ordered Soft Spheres. *J. Phys. Chem. B* **1998**, *102*, 8379–8388.
- (17) Wang, Z. L. Structural Analysis of Self-Assembling Nanocrystal Superlattices. *Adv. Mater.* **1998**, *10*, 13–30.
- (18) Murray, C. B.; Sun, S.; Gaschler, W.; Doyle, H.; Betley, T. A.; Kagan, C. R. Colloidal Synthesis of Nanocrystals and Nanocrystal Superlattices. *IBM J. Res. Dev.* **2001**, *45*, 47–56.
- (19) Ariga, K.; Hill, J. P.; Lee, M. V.; Vinu, A.; Charvet, R.; Acharya, S. Challenges and Breakthroughs in Recent Research on Self-Assembly. *Sci. Technol. Adv. Mater.* **2008**, *9*, 1–96.
- (20) Luedtke, W. D.; Landman, U. Structure, Dynamics, and Thermodynamics of Passivated Gold Nanocrystallites and Their Assemblies. *J. Phys. Chem.* **1996**, *100*, 13323–13329.
- (21) Rabani, E.; Reichman, D. R.; Geissier, P. L.; Brus, L. E. Drying-Mediated Self-Assembly of Nanoparticles. *Nature* **2003**, *426*, 271–274.
- (22) Talapin, D. V.; Shevchenko, E. V.; Murray, C. B.; Titov, A. V.; Kral, P. Dipole–Dipole Interactions in Nanoparticle Superlattices. *Nano Lett.* **2007**, *7*, 1213–1219.
- (23) Min, Y.; Akbulut, M.; Kristiansen, K.; Golan, Y.; Israelachvili, J. The Role of Interparticle and External Forces in Nanoparticle Assembly. *Nat. Mater.* **2008**, *7*, 527–538.
- (24) Schapotschnikow, P.; Pool, R.; Vlugt, T. J. H. Molecular Simulations of Interacting Nanocrystals. *Nano Lett.* **2008**, *8*, 2930–2934.
- (25) Kinge, S.; Credo-Calama, M.; Reinhoudt, D. N. Self-Assembling Nanoparticles at Surfaces and Interfaces. *Chem. Phys. Chem.* **2008**, *9*, 20–42.
- (26) M.Bishop, K. J.; Wilmer, C. E.; Soh, S.; Grzybowski, B. A. Nanoscale Forces and Their Uses in Self-Assembly. *Small* **2009**, *5*, 1600–630.
- (27) Bigioni, T. P.; Lin, X. M.; Nguyen, T. T.; Corwin, E. I.; Witten, T. A.; Jaeger, H. M. Kinetically Driven Self Assembly of Highly-Ordered Nanoparticle Monolayers. *Nat. Mater.* **2006**, *5*, 265–270.
- (28) Tang, Z. Y.; Zhang, Z. L.; Wang, Y.; Glotzer, S. C.; Kotov, N. A. Self-Assembly of CdTe Nanocrystals into Free-Floating Sheets. *Science* **2006**, *314*, 274–278.

- (29) Klecha, E.; Ingert, D.; Walls, M.; Pilani, M. P. Immunity of Coated Self-Ordered Silver Nanocrystals: A New Intrinsic Property Due to the Nanocrystal Ordering. *Langmuir* **2009**, *25*, 2824–2830.
- (30) Lisiecki, I.; Turner, S.; Balls, S.; Pilani, M. P.; Van Tendeloo, G. The Remarkable and Intriguing Resistance to Oxidation of 2D Ordered hcp Co Nanocrystals. A New Intrinsic Property. *Chem. Mater.* **2009**, *21*, 2335–2338.
- (31) Lisiecki, I.; Walls, M.; Parker, D.; Pilani, M. P. 2D Self-Organization of Core/Shell Cohcp/Co Nanocrystals. *Langmuir* **2008**, *24*, 4295–4299.
- (32) The d_{p-p} values in each of the three directions, for both arrays, are deduced from $d_{p-p} = (L - xD)/(x - 1)$, where L is the length of 20–25 minimum well-aligned nanocrystals (measurements made in area 1) or of 10–15 maximum well-aligned nanocrystals (measurements made in area 2). D is the diameter of the aligned nanocrystals, and x is the number of nanocrystals forming the line L. Note that L values are smaller in area 2 due to network defects and distortions involving fewer well-aligned nanocrystals than those in 1. The mean distance is the average of the three d_{p-p} related to the three hexagonal directions.
- (33) Donnet, J. B.; Custodero, E. STM Characterization of HOPG Surface Defects. *C.R. Acad. Sci. Paris* **1994**, *319*, 17–24.
- (34) Mekhalif, Z.; Laffineur, F.; Couturier, N.; Delhalle, J. Elaboration of Self-Assembled Monolayers of *n*-Alkanethiols on Nickel Polycrystalline Substrates: Time, Concentration, and Solvent Effects. *Langmuir* **2003**, *19*, 637–645.
- (35) Mamdouh, W.; Ji-I, H. U.; Ladislaw, J. S.; Dulcey, A. E.; Percec, V.; De Shryver, F. C.; De Feyter, S. Solvent Controlled Self-Assembly at the Liquid–Solid Interface Revealed by STM. *J. Am. Chem. Soc.* **2006**, *128*, 317–325.
- (36) Klecha, E.; Ag–C₁₀/Hexane, Ag–C₁₀/Decane, Ag–C₁₀/Dodecane and, Ag–C₁₂/Hexane, Ag–C₁₀/Octane, Ag–C₁₂/Decane and Ag–C₁₂/Dodecane; Intrinsic Properties of Silver Nanocrystals: Stability and Non Oxidation Against Oxygen Plasma; Ph.D. Thesis, UPMC, 2009.
- (37) Martin, J. E.; Wilcoxon, J. P.; Odinek, J.; Provencio, P. Control of the Interparticle Spacing in Gold Nanoparticle Superlattices. *J. Phys. Chem. B* **2000**, *104*, 9475–9486.
- (38) Cölfen, H.; Mann, S. Higher-Order Organization by Mesoscale Self-Assembly and Transformation of Hybrid Nanostructures. *Angew. Chem., Int. Ed.* **2003**, *42*, 2350–2365.
- (39) If we take into account the procedure used to disperse the nanocrystals in octane, decane, and dodecane (i.e., evaporation of the hexane from the mother solution and then dispersion in an other solvent), this could be attributed to the fact that some hexane molecules remain strongly adsorbed on the thiol chains. For any used coating agent, the nanocrystals previously dispersed in hexane are entirely dispersed in octane after hexane evaporation, while the amount of nanocrystals is rather low when dispersed in decane and dodecane. This indicates that the increase in the number of carbon atoms in the solvent hydrocarbon chain decreases the nanocrystals solubility, which is related to the fact that larger solvent molecules cannot easily penetrate into the coating chains' corona. The dispersion in the other solvents involves a competition between the hexane molecules already adsorbed and the adsorption of the “new” solvent molecules (octane, decane, or dodecane) coming from the bulk phase, leading to the replacement of some hexane ones. The affinity between the coating and solvent tails increases upon increasing the solvent length, which improves the thiol tails' organization and induces, therefore, a greater permeation of the soft coronas to reach a maximum. A further increase in the solvent length reduces the permeation due to the adsorption of larger solvent molecules on the thiol tails.
- (40) Pradeep, T.; Mitra, S.; Sreekumaran Nair, A.; Mukhopadhyay, R. Dynamics of Alkyl Chains in Monolayer Protected Au and Ag Clusters and Silver thiolates: A Comprehensive QENS Investigation. *J. Phys. Chem. B* **2004**, *108*, 7012–7020.
- (41) Landman, U.; Luedtke, W. D. Small is Different: Energetic, Structural, Thermal, and Mechanical Properties of Passivated Nanocluster Assemblies. *Faraday Discuss.* **2004**, *125*, 1–22.
- (42) Jiang, Z.; Lin, X. M.; Sprung, M.; Narayanan, S.; Wang, J. Capturing the Crystalline Phase of Two-Dimensional Nanocrystal Superlattices in Action. *Nano Lett.* **2010**, *10*, 799–803.
- (43) Bormashenko, E. Wetting of Flat and Rough Curved Surfaces. *J. Phys. Chem. C* **2009**, *113*, 17275–17277.
- (44) Taleb, A.; Petit, C.; Pilani, M. P. Synthesis of Highly Mono-disperse Silver Nanoparticles from AOT Reverse Micelles: A Way to 2D and 3D Self-Organization. *Chem. Mater.* **1997**, *9*, 950–959.
- (45) Courty, A.; Lisiecki, I.; Pilani, M. P. Vibration of Self-Organized Silver Nanocrystals. *J. Chem. Phys.* **2002**, *116*, 8074–8078.